Supporting Information

Targeted Biomimetic Stem Cell Membrane–Exosome Composite Delivery System for the Treatment of Bone Defects

Chong Yin [1,2,§], Jinshu Yu [1,2,3,§], Hongwei Pang [1,2], Min Xu [1,2], Binxin Wang [1,2], Wei Chen [4], Ning Xie [1,2,], Bin Guo [1,2,*]*

1 Department of Clinical Laboratory, Affiliated Hospital of North Sichuan Medical College, Nanchong 637000, China

2 School of Laboratory Medicine, Translational Medicine Research Center, North Sichuan Medical College, Nanchong 637000, China

3 Department of Clinical Laboratory, Santai County People's Hospital, Mianyang 621000, China

4 Xinjiang Hua Shidan Drug Research Co., LTD, Urumqi, 830011, China

§ These authors contributed equally to this work.

* Corresponding author

E-mail: Ning Xie*:* xiening19840820@163.com; Bin Guo: guobin1368@163.com

Supplementary Figures:

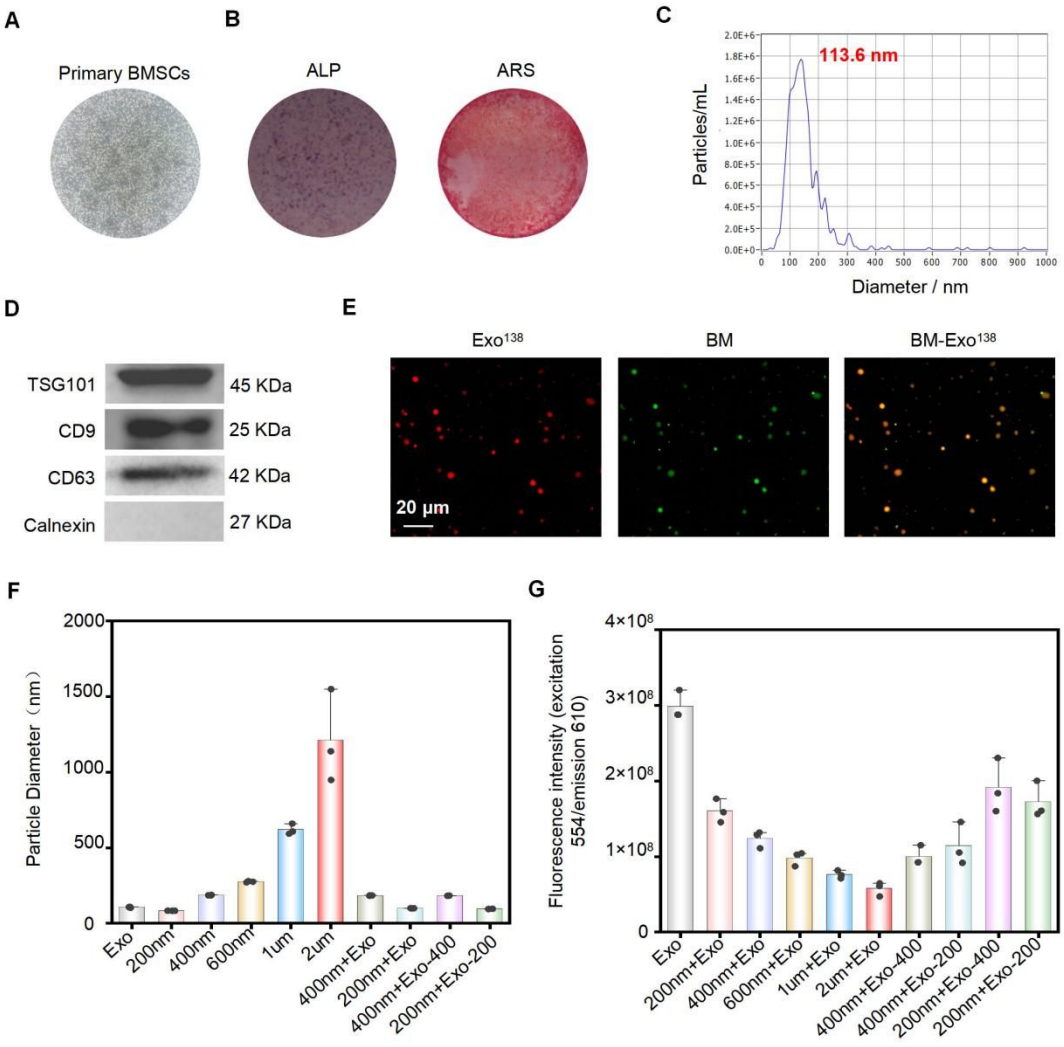

Figure S1. BMSCs and Exo^{138} characterization. A) Morphological characterization of BMSCs primary cells. B) Representative images of ALP and ARS staining after osteogenic differentiation-induced BMSCs. C) NTA assay for size distribution and concentration. D) Western blot analysis of exosome characterization marker proteins such as TSG101, CD9, CD63 and Calnexin. E) Exo^{138} labeled with red fluorescent DiI and BM labeled green fluorescent DiO, Confocal fluorescence image for co-localization analysis. Scale bar of: 20 um. F) and DiI fluorescence intensity.G) of BM-Exo^{138} vesicles under different pore sizes and procedures. Exo: naked exosomes. 200nm, 400nm, 600nm, 1um, 2um: BMSC membrane vesicles under different pore sizes. 200nm+Exo, 400nm+Exo, 600nm+Exo, 1um+Exo, 2um+Exo: exosomes encapsulated by BMSC membrane vesicles under different pore sizes. 200nm+Exo-200, 400nm+Exo-400, 200nm+Exo-200, 400nm+Exo-400: exosomes

encapsulated by BMSC membrane vesicles under different pore sizes, then followed another polycarbonate membrane with different pore size.

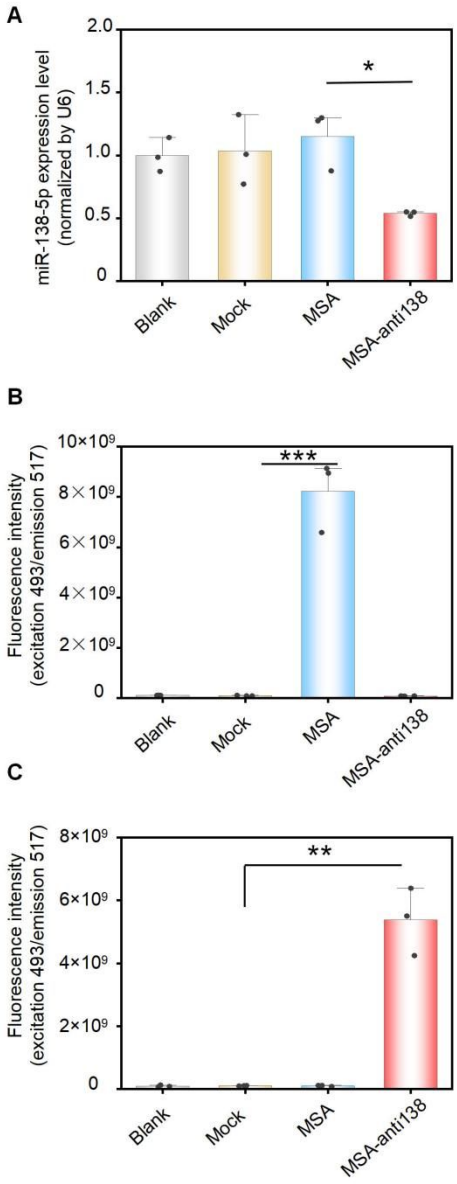

Figure S2. Evidence of the presence of MSA-anti-138 in exosomes. A) Expression of miR-138-5p in MC3T3-E1 cells transfected with MSA-anti-138. B) Fluorescence intensity of FAM in exosomes isolated from FAM labeled MSA transfected MC3T3-E1 cells, with unlabeled MSA-anti-138 as control. C) Fluorescence intensity of FAM in exosomes isolated from FAM labeled MSA-anti-138 transfected MC3T3-E1 cells, with unlabeled MSA as control. $*p < 0.05$, $**p < 0.01$, $***p < 0.001$.

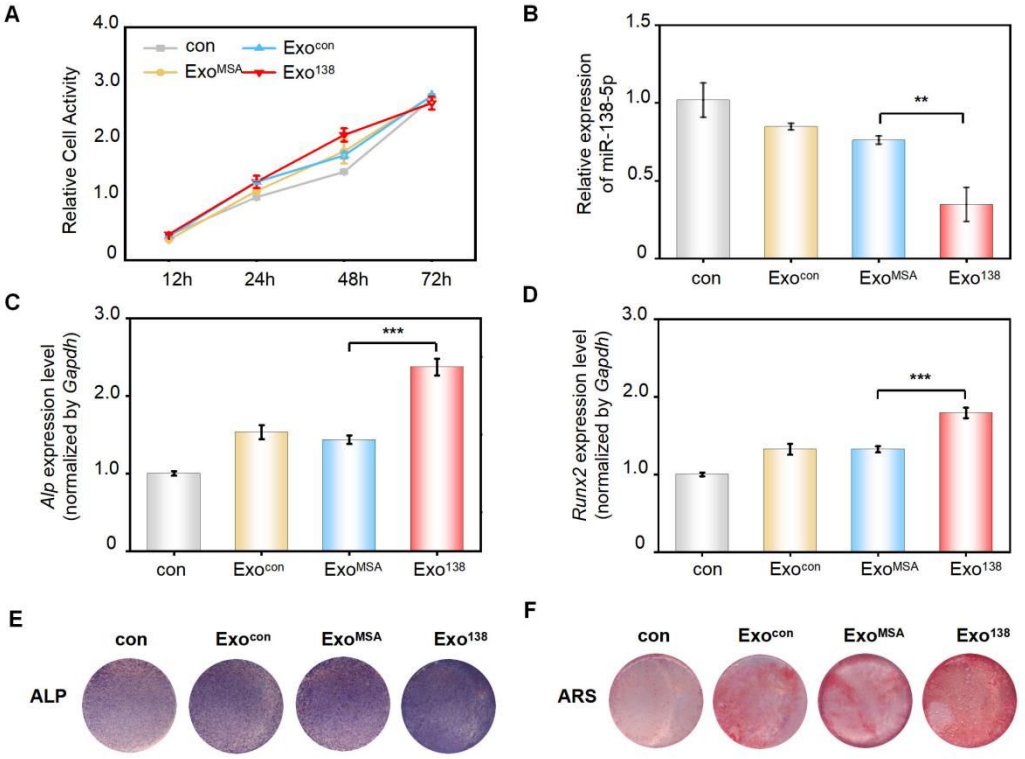

Figure S3. Effects of Exo^{138} on the regulation of osteogenic differentiation in vitro. A) CCK-8 assay. B) Expression of gene miR-138-5p. C, D) Expression levels of osteogenic genes *Alp* and *Runx2*. E, F) Representative images of ALP and ARS staining. *p < 0.05, **p < 0.01, ***p < 0.001, and ns indicating non-significant differences.

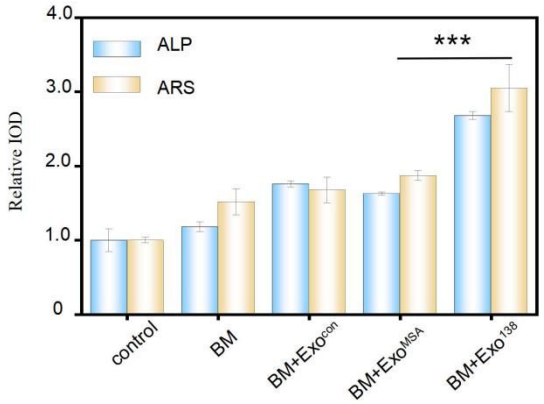

Figure S4. Quantitative analysis of ALP and ARS staining results in Figure 3C. ***p < 0.001.

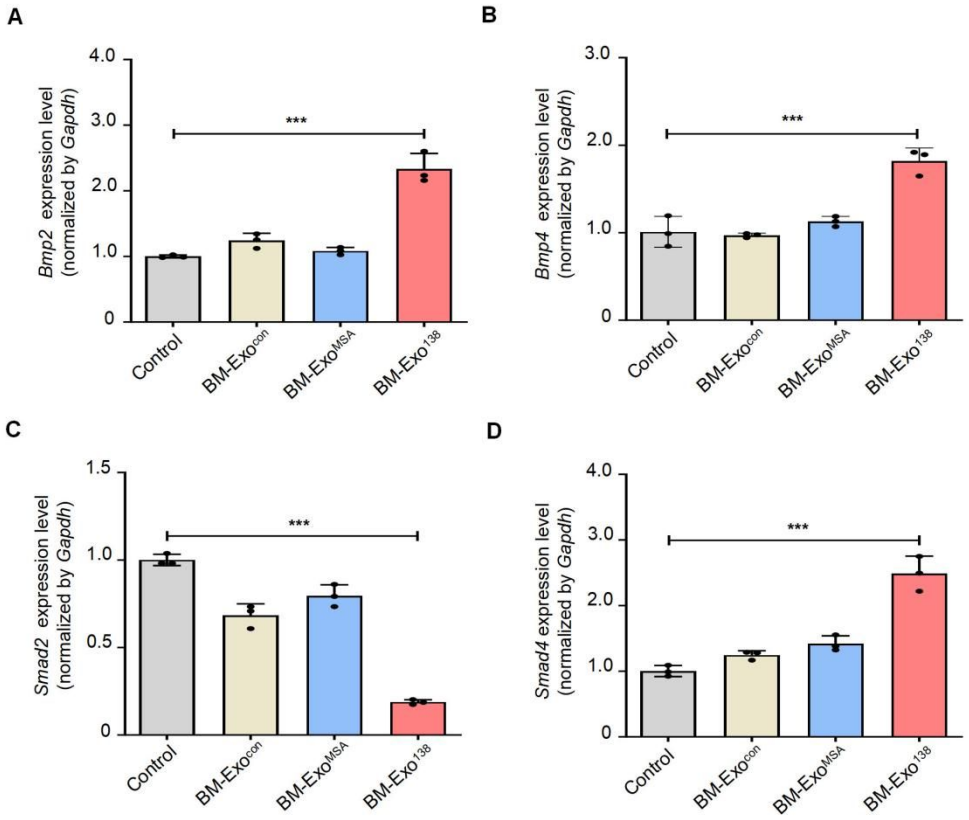

Figure S5. PT-PCR of genes expression of key regulators of TGF-β pathway after co-incubation by each group. *$p < 0.05$, **$p < 0.01$, ***$p < 0.001$, and ns indicating non-significant differences.

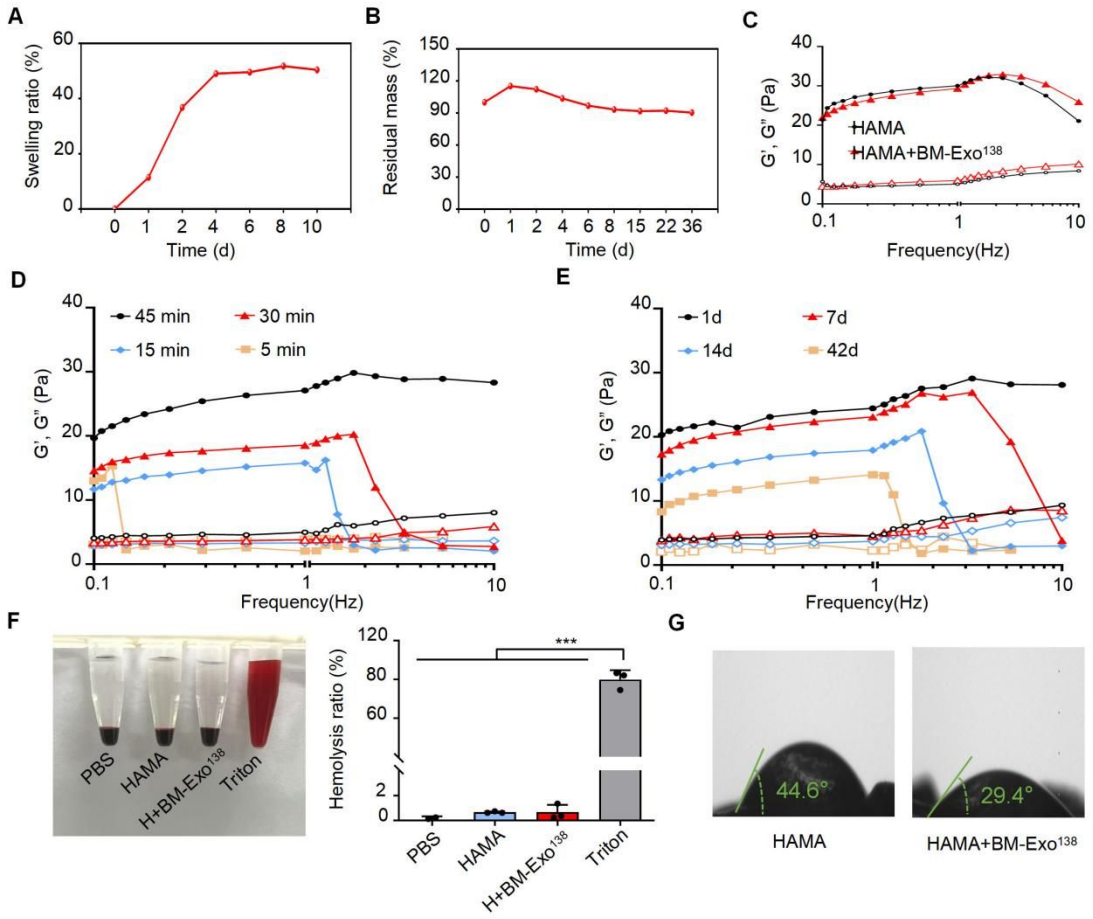

Figure S6. HAMA+BM-Exo^{138} characterization. A) Swelling rate. B) Degradation curve. C) Rheological behavior. D) Gelation time of HAMA hydrogel. E) In vitro degradation kinetics of HAMA hydrogel. F) Hemolytic picture and Hemolysis rate. G) Water contact angle. *p < 0.05, **p < 0.01, ***p < 0.001, and ns indicating non-significant differences.

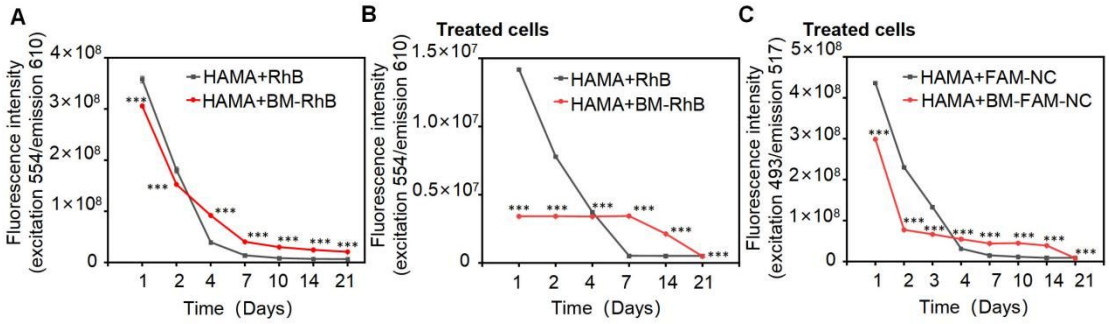

Figure S7. A, B) Comparison of the slow-release of HAMA encapsulated Rhodamine B and BM-Rhodamine B. ***p < 0.001. C) Comparison of the slow-release of HAMA encapsulated FAM-NC and BM-FAM-NC. ***p < 0.001.

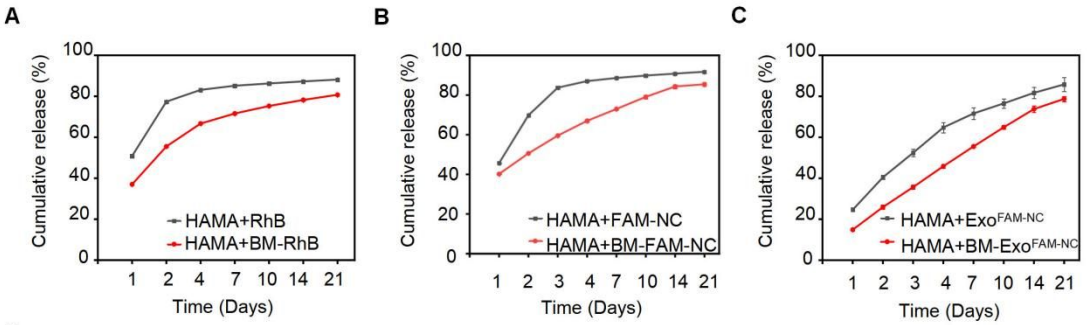

D

	Zero-order equation		First-order equation		Higuchi equation	
	K_0	R^2	K_1	R^2	K_H	R^2
HAMA+Exo^{FAM-NC}	2.61	0.7031	-0.07982	0.8614	16.09	0.8483
HAMA+BM-Exo^{FAM-NC}	3.035	0.8387	-0.06983	0.9241	18.13	0.9453

Figure S8. Release kinetics and biocompatibility analysis of HAMA. A-C)In vitro cumulative release profiles. D) Kinetic parameters of three equations (zero-order equation, first-order equation and Higuchi equation) in fitting the release data of Exo^{FAM-NC} /BM-Exo^{FAM-NC} from HAMA hydrogel. K represented the rate of release, R2evaluated the fitness of equation in fitting data.

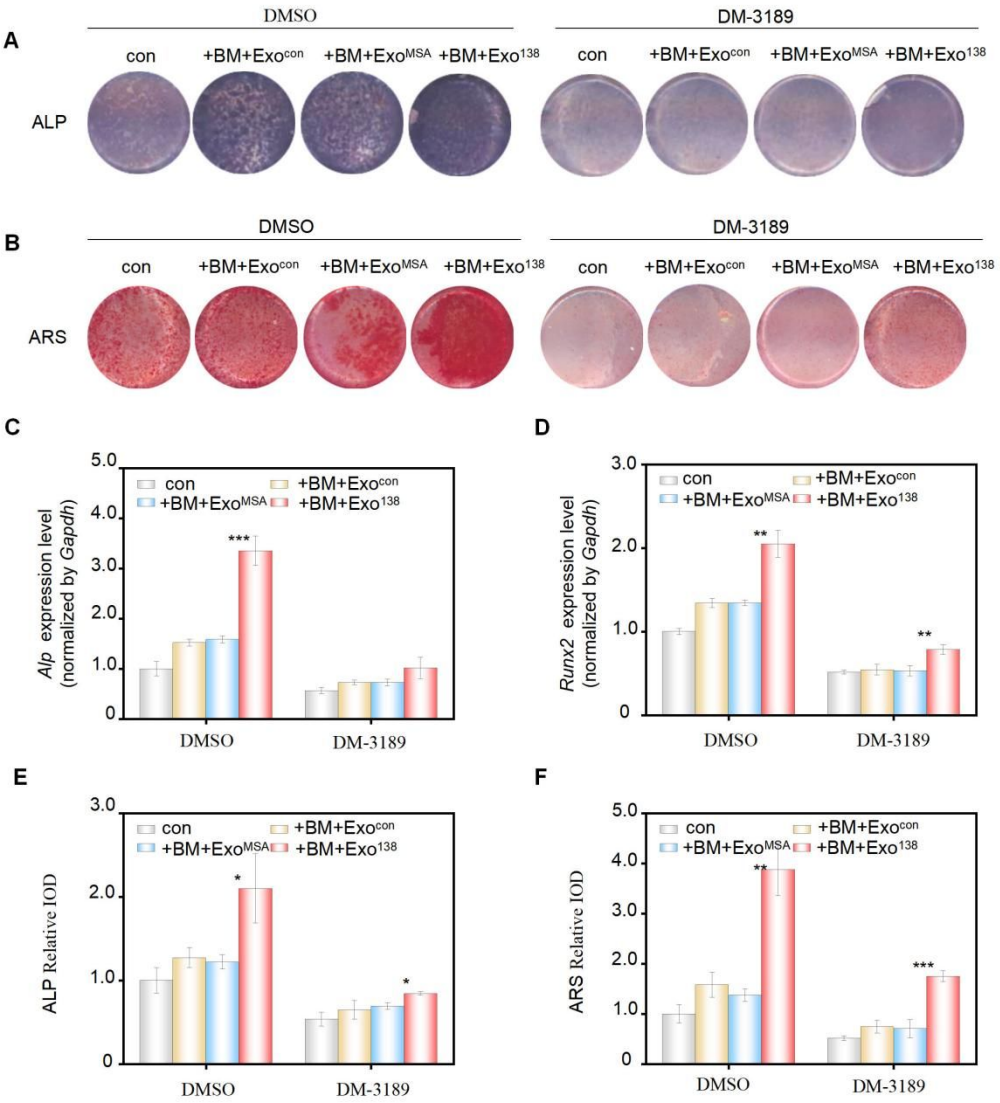

Figure S9. Effects of BM-Exo^{138} on osteogenic differentiation after using TGF-β/BMP inhibitor. A, B) ALP and ARS staining of MC3T3-E1 cells treated with BM－Exo138 in the absence of DMSO or NC043; C, D) Alp and Runx2 mRNA expression levels of MC3T3-E1 cells treated with BM－Exo^{138} in the absence of DMSO or NC043. E, F) quantitative analysis is required for the ALP and ARS staining. *$p < 0.05$, **$p < 0.01$, ***$p < 0.001$.

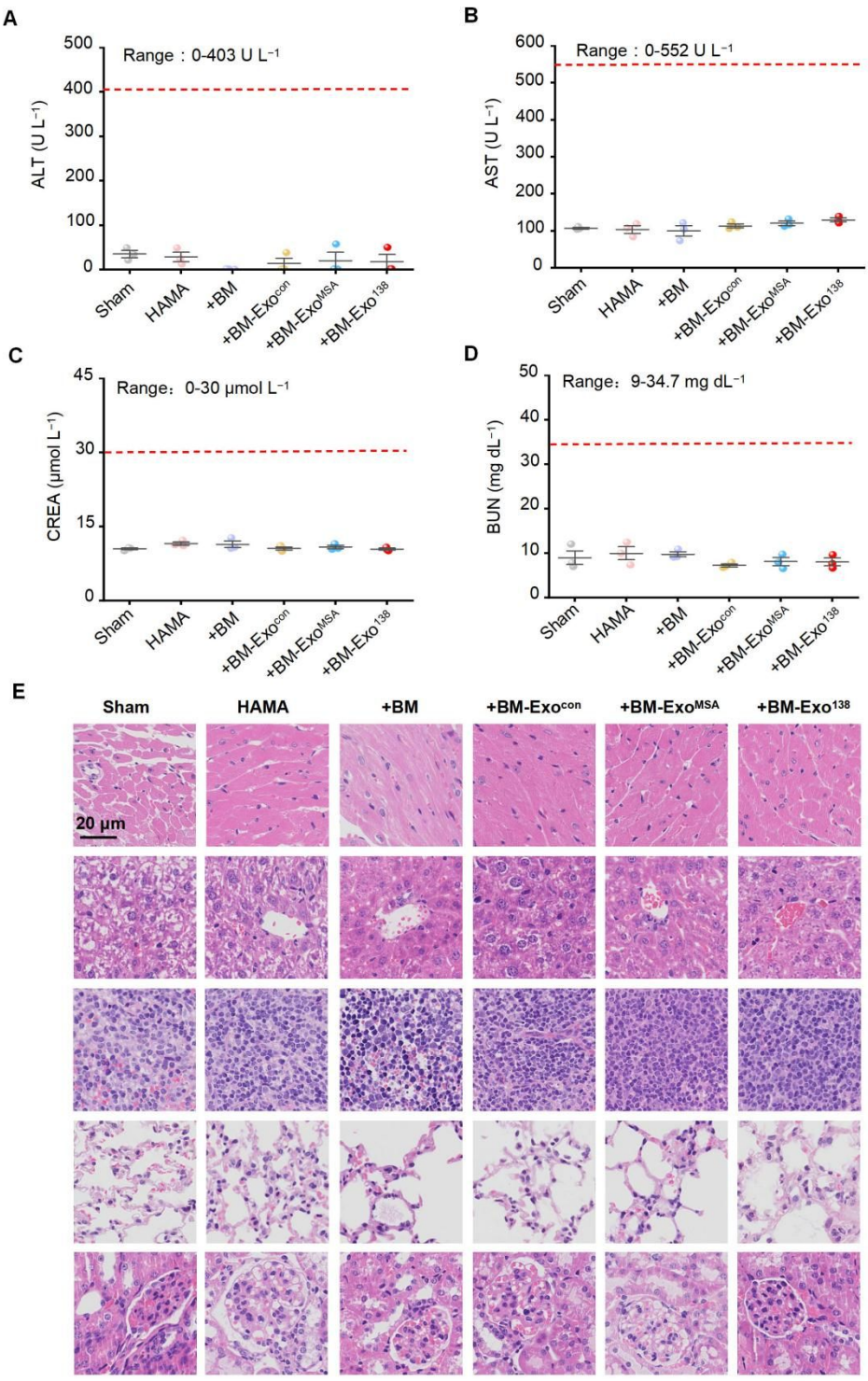

Figure S10. Biocompatibility of HAMA+BM-Exo^{138} in vivo . A-D) Blood chemistry markers in mice, including alanine aminotransferase (ALT), aspartate aminotransferase (AST), creatinine (Cr), and blood urea nitrogen (BUN). E) H&E staining of tissue samples. Blood and major organs were collected from bone-deficient mice implanted with different hydrogel compositions. Scale bar: 20 μm.

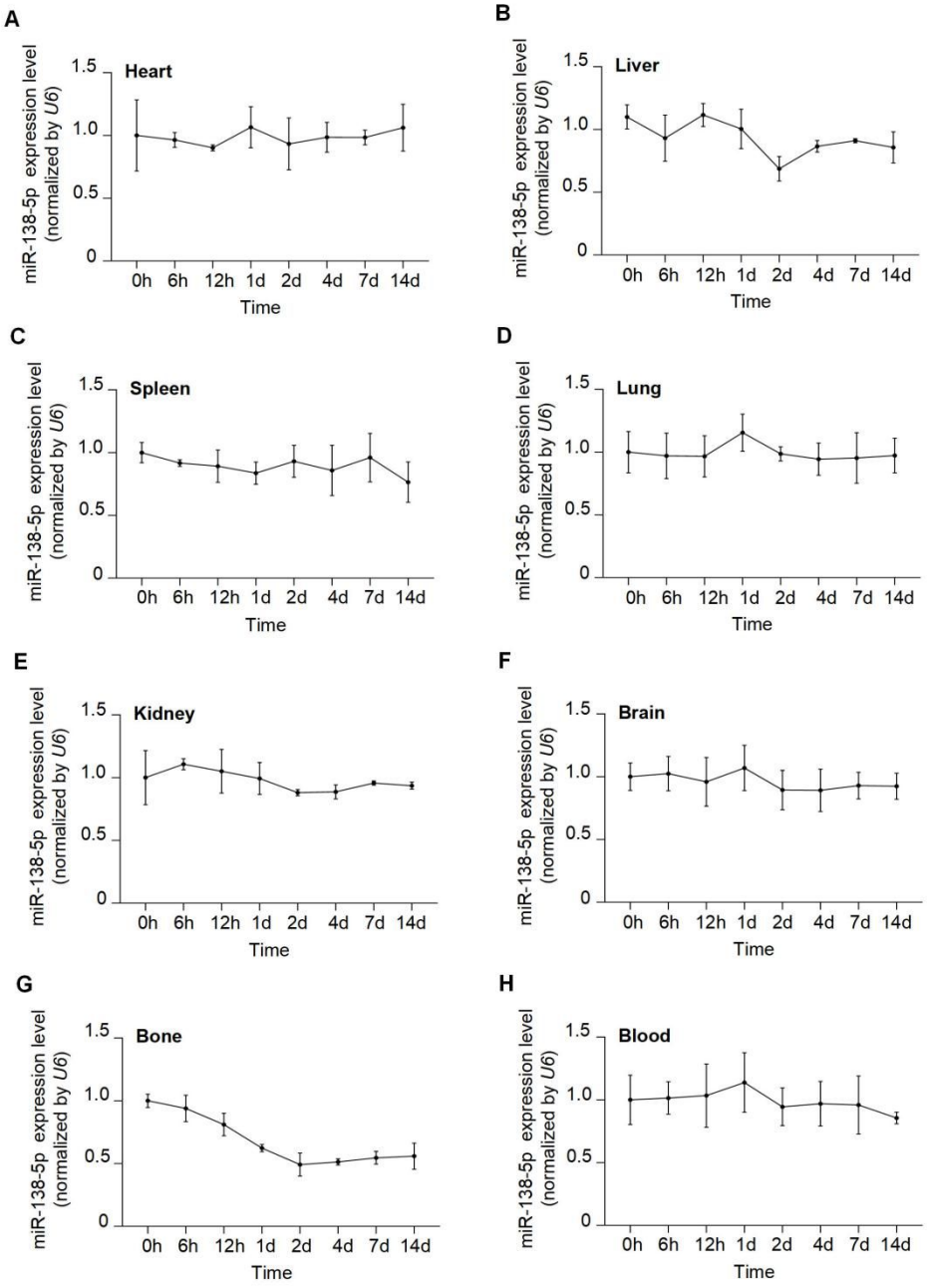

Figure S11. Pharmacokinetics of MSA-antago-138. A-H) miR-138-5p expression levels in different organs were detected using stem-loop RT-PCR at the indicated time intervals after implantation of HAMA+BM-Exo^{138} hydrogel.

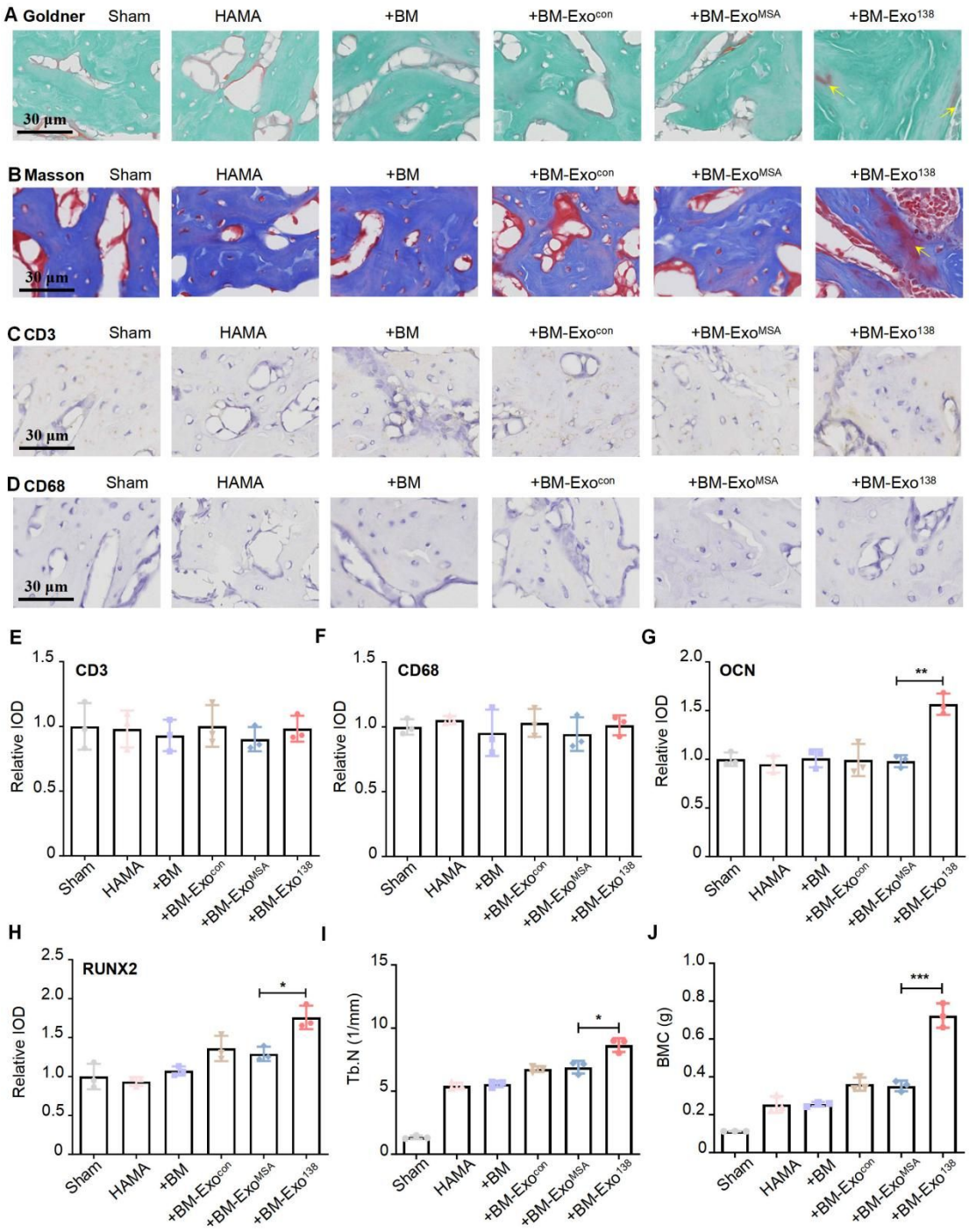

Figure S12. Effects of HAMA+BM-Exo^{138} on in situ bone regeneration, inflammation, and osteogenic differentiation in tibial defect mice. A) Goldner's trichrome staining of tibial defect regions (Scale bar: 30 μm; Magnification: ×400). B) Masson's trichrome staining of tibial defect regions (Scale bar: 30 μm; Magnification: ×400). C-F) Immunohistochemical images of inflammatory factors cluster of differentiation CD3 (C) and CD68 (D) in tibial defect regions, and quantification of corresponding integrated optical density (IOD) (scale bar: 30 μm; magnification:

×400). G, H) Osteocalcin (OCN) and Runt-related transcription factor 2 (RUNX2) staining images quantification of corresponding IOD I, J). Statistical analysis of microCT of proximal tibia Tb.N and BMC after different hydrogel treatments. *p < 0.05, **p < 0.01, ***p < 0.001, and ns indicating non-significant differences.

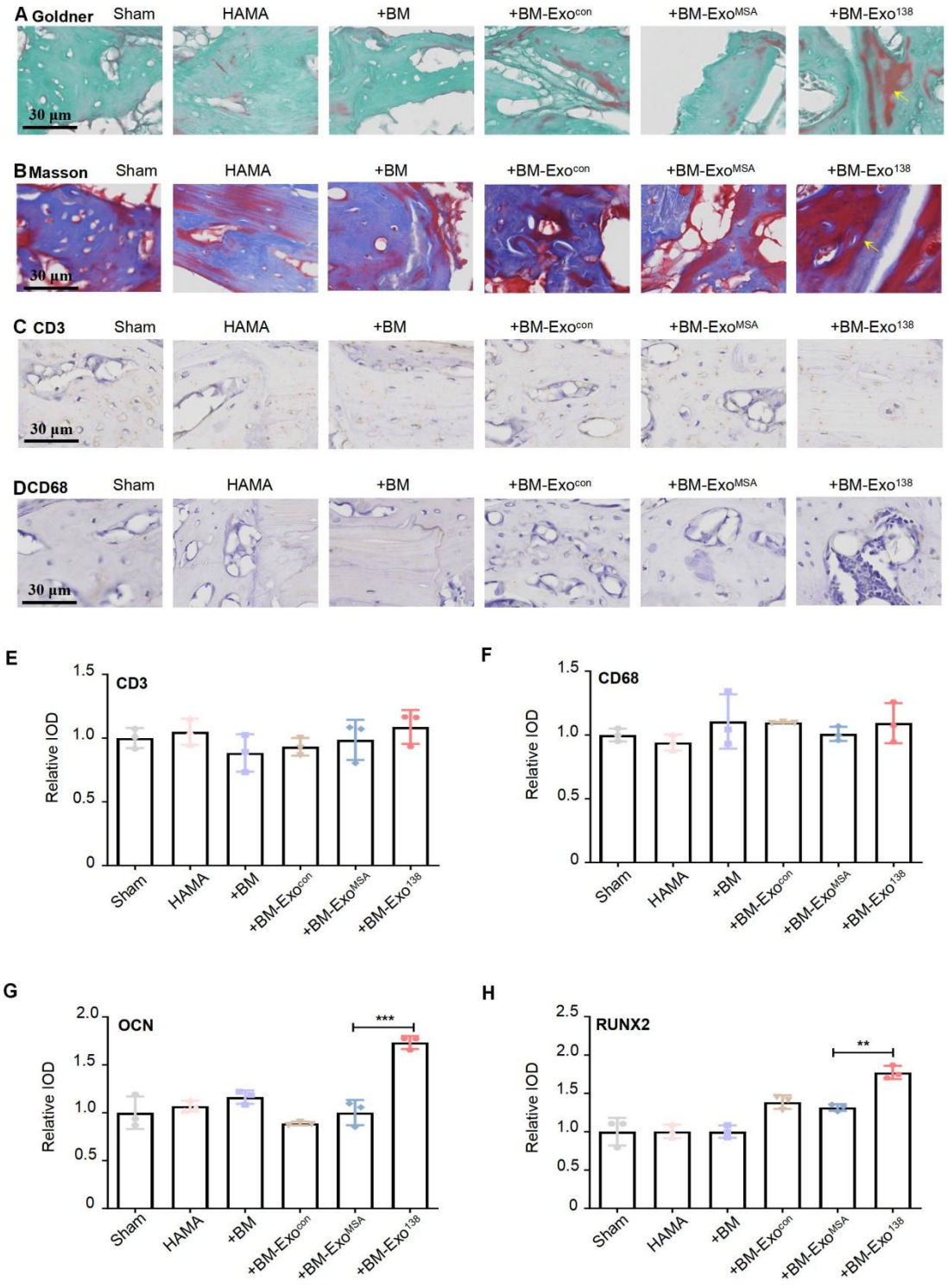

Figure S13. Effects of HAMA+BM-Exo^{138} on in situ bone regeneration, inflammation, and osteogenic differentiation in calvarial defect mice. A) Goldner's trichrome staining of tibial defect regions (Scale bar: 30 μm; Magnification: ×400). B) Masson's trichrome staining of tibial defect regions (Scale bar: 30 μm; Magnification: ×400). C-F) Immunohistochemical images of inflammatory factors cluster of differentiation CD3 (C) and CD68 (D) in tibial defect regions, and quantification of

corresponding integrated optical density (IOD) (scale bar: 30 μm; magnification: ×400). G, H) Osteocalcin (OCN) and Runt-related transcription factor 2 (RUNX2) staining images quantification of corresponding IOD. *$p < 0.05$, **$p < 0.01$, ***$p < 0.001$, and ns indicating non-significant differences.

Supplementary Table:

Table S1. Primer Sequences of RT-PCR.

Target gene	Sequences (5’→3’)
miRa)-138-5p-forward	GGCAGCTGGTGTTGTGAATC
miR-138-5p-reverse	ACTGCAGGGTCCGAGGTATT
miR-138-5p-RTb)	GTCGTATCGACTGCAGGGTCCGAGGTATTCGCAGTCGATACGACCGGCCT
Alp-forward	GGCCATTGGCACCTGCCTTA
Alp-reverse	ACCCATCCCATCTCCCAGGAA
Runx2-forward	TCTGGCCTTCCACTCTCAGT
Runx2-reverse	GACTGGCGGGGTGTAAGTAA
Bmp2-forward	ACTTTTCTCGTTTGTGGAGC
Bmp2-reverse	GAACCCAGGTGTCTCCAAGA
Bmp4-forward	GAGGAGGAGGAAGAGCAGAG
Bmp4-reverse	TGGGATGTTCTCCAGATGTT
Smad2-forward	CCATCCCCGAGAACACTAACTT
Smad2-reverse	TGGTGGTCGCTAGTTTCTCCAT
Smad4-forward	ACGAACGAGTTGTATCACCTGG
Smad4-reverse	ATGGCTGTCCCTCAAAGTCAT
U6-Forward	GTGCTCGCTTCGGCAGCACATAT
U6-Reverse	AAAATATGGAACGCTTCACGAA
U6-RT	AACGCTTCACGAATTTGCGT
Gapdh-forward	CATGGAGAAGGCTGGGGCTC
Gapdh-reverse	CACTGACACGTTGGCAGTGG

[a)] miR: miRNA; [b)] RT: reverse transcript